J|A|C|S ARTICLES

Published on Web 11/24/2009

Residue-Specific Information about the Dynamics of Antimicrobial Peptides from $^{1}H-^{15}N$ and ^{2}H Solid-State NMR Spectroscopy

Kresten Bertelsen,[†] Berit Paaske,[†] Lea Thøgersen,[†,‡] Emad Tajkhorshid,[§] Birgit Schiøtt,[†] Troels Skrydstrup,[†] Niels Chr. Nielsen,[†] and Thomas Vosegaard*[,†]

Center for Insoluble Protein Structures (inSPIN), Interdisciplinary Nanoscience Center (iNANO), and Department of Chemistry, Bioinformatics Research Center, University of Aarhus, DK-8000 Aarhus C, Denmark, and Department of Biochemistry and Beckman Institute, University of Illinois at Urbana−Champaign, 405 North Mathews, Urbana, Illinois 61801

Received July 3, 2009; Revised Manuscript Received October 9, 2009; E-mail: tv@chem.au.dk

Abstract: We present a new method to obtain information about the conformational dynamics of membrane-proteins using solid-state NMR experiments of oriented samples. By measuring the orientation-dependent $^{1}H-^{15}N$ dipole−dipole coupling, ^{15}N anisotropic chemical shift, and ^{2}H quadrupole coupling parameters for a single residue, it is possible to obtain information about the local dynamics of each residue in the protein. This may be interpreted on an individual basis or through models extended to study conformational motion of membrane-protein segments. The method is demonstrated for the antimicrobial peptaibol alamethicin for which combined analysis of anisotropic interactions for the Aib_8 residue provides detailed information about helix-tilt angle, wobbling, and oscillatory rotation around the helix axis in the membrane bound state. This information is in very good agreement with coarse-grained MD simulations of the peptide in lipid bilayers.

Introduction

Oriented-sample solid-state NMR spectroscopy has proven to be a powerful tool to determine the structure and conformation of membrane proteins within phospholipid bilayer membranes.[1−3] The method relies on the measurement of orientation-dependent anisotropic parts of nuclear spin interactions providing detailed information about the orientation of, for example, peptide planes relative to the magnetic field and thereby the membranes of the oriented sample. Typically, the experimental data have been interpreted under the assumption that the protein adopts a single well-defined structure and conformation within the hydrophobic framework of the lipids, characterized, for example, by so-called PISA-wheel resonance patterns in 2D separated-local-field (SLF) experiments or ^{2}H quadrupolar coupling variations.[2,4] This assumption is, however, not always true, and recent studies report on flexibility and extensive conformational dynamics, for example, for peptide ion channels.[5−9] In the limit of fast axial motion around the bilayer normal, the rotational dynamics may be described by an order parameter for the bilayer/bicelle motion, which is typically measured from ^{31}P or ^{2}H experiments on oriented phospholipid bilayers.[6]

Focusing on small antimicrobial peptides such as peptaibols, which currently attract great interest as peptide alternatives to small-molecule antibiotics, their mechanism of action is still not well understood. In addition to a number of structural studies of the peptaibol alamethicin embedded in phospholipid bilayers,[3,9−12] we have recently reported that the membrane-bound conformation of alamethicin is highly dynamic, as determined using a combination of micelle liquid-state NMR

[†] Center for Insoluble Protein Structures (inSPIN), Interdisciplinary Nanoscience Center (iNANO), and Department of Chemistry, University of Aarhus.

[‡] Bioinformatics Research Center, University of Aarhus.

[§] University of Illinois at Urbana−Champaign.

(1) (a) Bechinger, B.; Kim, Y.; Chirlian, L. E.; Gesell, J.; Neumann, J. M.; Montal, M.; Tomich, J.; Zasloff, M.; Opella, S. J. *J. Biomol. NMR* **1991**, *1*, 167. (b) Opella, S. J. *Nat. Struct. Biol.* **1997**, *4*, 845.

(2) (a) Wang, J.; Denny, J.; Tian, C.; Kim, S.; Mo, Y.; Kovacs, F.; Song, Z.; Nishimura, K.; Gan, Z.; Fu, R.; Quine, J. R.; Cross, T. A. *J. Magn. Reson.* **2000**, *144*, 162. (b) Marassi, F. M.; Opella, S. J. *J. Magn. Reson.* **2000**, *144*, 150.

(3) Bak, M.; Bywater, R. P.; Hohwy, M.; Thomsen, J. K.; Adelhorst, K.; Jakobsen, H. J.; Sørensen, O. W.; Nielsen, N. C. *Biophys. J.* **2001**, *81*, 1684.

(4) (a) Marassi, F. M. *Biophys. J.* **2001**, *80*, 994. (b) Vosegaard, T.; Nielsen, N. C. *J. Biomol. NMR* **2002**, *22*, 225.

(5) Nevzorov, A. A.; Moltke, S.; Heyn, M. P.; Brown, M. F. *J. Am. Chem. Soc.* **1999**, *121*, 7636.

(6) Nevzorov, A. A.; De Angelis, A. A.; Park, S. H.; Opella, S. J. In *NMR Spectroscopy of Biological Solids*; Ramamoorthy, A., Ed.; Taylor & Francis: New York, 2005; p 177.

(7) Park, S. H.; Mrse, A. A.; Nevzorov, A. A.; De Angelis, A. A.; Opella, S. J. *J. Magn. Reson.* **2006**, *178*, 162.

(8) Page, R. C.; Kim, S.; Cross, T. A. *Structure* **2008**, *16*, 787.

(9) Dittmer, J.; Thøgersen, L.; Underhaug, J.; Bertelsen, K.; Vosegaard, T.; Pedersen, J. M.; Schiøtt, B.; Tajkhorshid, E.; Skrydstrup, T.; Nielsen, N. C. *J. Phys. Chem. B* **2009**, *113*, 6928.

(10) (a) Bechinger, B.; Skladnev, D. A.; Ogrel, A.; Li, X.; Rogozhkina, E. V.; Ovchinnikova, T. V.; O'Neil, J. D.; Raap, J. *Biochemistry* **2001**, *40*, 9428. (b) Salnikov, E. S.; Friedrich, H.; Li, X.; Bertani, P.; Reissmann, S.; Hertweck, C.; O'Neil, J. D. J.; Raap, J.; Bechinger, B. *Biophys. J.* **2009**, *96*, 86.

(11) Bertelsen, K.; Pedersen, J. M.; Rasmussen, B. S.; Skrydstrup, T.; Nielsen, N. C.; Vosegaard, T. *J. Am. Chem. Soc.* **2007**, *129*, 14717.

(12) Vosegaard, T.; Bertelsen, K.; Pedersen, J. M.; Thøgersen, L.; Schiøtt, B.; Tajkhorshid, E.; Skrydstrup, T.; Nielsen, N. C. *J. Am. Chem. Soc.* **2008**, *130*, 5028.

and molecular-dynamics (MD) simulations.[9,13] These observations are not consistent with a single well-defined conformation of alamethicin in the membrane and provide new experimental evidence that alamethicin samples many conformational states including a variety of channel-forming oligomers with different ion conductance.[14] Overall such observations are not consistent with a single well-defined conformation where the system can be described simply in terms of an overall order parameter for the membranes and a simple structure of the peptide. We have recently investigated the static disorder of alamethicin, which may be explained by a combination of peptide and lipid disorder.[12,13] However, it is obvious that a characterization of the static distribution of molecular conformations does not probe the flexibility of the peptide and peptide−lipid anchoring. This flexibility calls for methods enabling detailed studies of the peptide structure and dynamics in the membrane environment. Following this approach, recent studies have addressed the detection of fast dynamics in peptide/protein membrane anchoring that leads to an averaging of the nuclear spin interactions over the conformational space adopted by the molecule due to the dynamics,[8,15] by simultaneously observing the deviations from resonance patterns observed for several residues throughout the entire peptide chain in peptides assumed to be in ideal α-helical structures. This provides "rigid-body" information about the conformational dynamics of structural elements such as α-helices, which are themselves assumed to be stiff rods.

In this Article, we pursue a different approach and propose a method whereby we can measure the dynamics of individual residues, which may be used to probe the conformational dynamics on the level of the individual residue. Ultimately, by accumulating the conformational and dynamic information for all residues, such analyses may provide very detailed information about both the overall dynamics of the peptide and the local variations in dynamics throughout the peptide chain. Alternatively, the technique may be used to describe the conformation and segmental motion of a full peptide or a fragment of a peptide, as, for example, a helical element of a membrane spanning peptide. Without resorting to uniformly isotope-labeled samples or many samples labeled on individual residues, we will in this first demonstration of the method stick to the latter approach and use the conformational restraints from several nuclear spin interactions within a single residue to determine the average conformation and segmental dynamics of a peptide segment of the membrane-spanning antimicrobial peptide alamethicin. We address particular focus on the central part of the peptide between the highly conserved Gln_7 residue, playing a key role in the conductance properties of alamethicin channels and the flexible hinge formed by Gly_{11} to Pro_{14}. We target this part of the molecule by investigating the conformation and dynamics of Aib_8 from combined analysis of data from the orientation-dependent ^{15}N chemical shift, $^1H-^{15}N$ dipole−dipole coupling, and ^2H quadrupole coupling interactions for this residue.[11,12]

Materials and Methods

Synthesis of ^{15}N- and ^2H-Labeled Peptides and Preparation of Solid-State NMR Samples. ^{15}N- and ^2H-labeled α-aminoisobutyric acid (Aib) was prepared and equipped with Fmoc protection groups as described previously starting from $^{15}NH_4Cl$ and deuterated acetone.[11,12] The amino acid sequence of alamethicin used in this work corresponds to alamethicin-F30: Ac-Aib-Pro-Aib-Ala-Aib_5-Ala-Gln-Aib*-Val-Aib_{10}-Gly-Leu-Aib-Pro-Val_{15}-Aib-Aib-Glu-Gln-$Phol_{20}$, which has the normal peptaibol characteristics with an acetylated (Ac) N-terminus and a phenylalaninol (Phol) alcohol at the C-terminus. The peptides were synthesized fully automated on a CEM microwave-assisted peptide synthesizer as described elsewhere,[16] and labeled with either ^{15}N or ^2H at residue Aib_8. In total, four different samples were prepared. Two samples consisting of lyophilized peptide labeled with either ^{15}N or ^2H at Aib_8 were used to assess the anisotropic parameters. The macroscopically aligned sample containing ^{15}N-Aib_8 alamethicin reconstituted in dimyristoylphosphatidylcholine (DMPC) for oriented-sample ^{15}N solid-state NMR was prepared by codissolving peptide and lipids in MeOH, distributing the mixture on glass slides, evaporation of organic solvent, and rehydration at 100% relative humidity as described in ref 12. The sample, consisting of 16 stacked glass plates, was placed in a sealed plastic bag with a piece of wet cloth to keep the hydration for several days. The DMPC vesicle-reconstituted ^2H-Aib_8 alamethicin sample in water for ^2H magic-angle spinning (MAS) NMR studies was prepared by adding peptide dissolved in minimal amounts of MeOH to a suspension DMPC in water, addition of water, lyophilization, and resuspension in water as described elsewhere.[11] For both lipid−peptide samples, the molar peptide:lipid ratio was 1:15.

Solid-State NMR Experiments. All solid-state NMR spectra were recorded on a Bruker-700 Avance-II wide-bore NMR spectrometer as described previously.[11,12] In brief, the ^2H MAS experiments employed a spin rate of 2000 Hz and single-pulse excitation (2 μs, 50 kHz radio frequency (rf) field strength) in a 4 mm Bruker MAS probe, while the oriented-sample ^{15}N CP experiments were performed in a Bruker flat-coil probe using either ^1H SPINAL-64[17] heteronuclear or FSLG[18] homonuclear decoupling during acquisition, both using ^1H rf field strengths of 65 kHz during the 5 ms acquisition time. All experiments were performed at 30 °C. ^{15}N and ^2H solid-state spectra of bilayer-reconstituted peptides, shown in Figure 1, allow measurement of the orientation-dependent ^{15}N chemical shift and ^2H quadrupolar coupling interactions scaled by dynamics of the peptide in its fluid membrane environment, respectively, while the spectra of the lyophilized powder samples (Figure 1e,f) serve to measure the unscaled interactions (vide infra).

All spectra were processed using Bruker Topspin (Bruker, Rheinstetten), while all numerical simulations were performed using the SIMPSON[19,20] and SIMMOL[20,21] open-source software packages.

Interpretation of the Solid-State NMR Experiments. The Hamiltonian describing the relevant nuclear spin interactions for

(13) Thøgersen, L.; Schiøtt, B.; Vosegaard, T.; Nielsen, N. C.; Tajkhorshid, E. *Biophys. J.* **2008**, *95*, 4337.
(14) (a) Latorre, R.; Miller, C. G.; Quay, S. *Biophys. J.* **1981**, *36*, 803. (b) Hall, J. E.; Vodyanoy, I.; Balasubramanian, T. M.; Marshall, G. R. *Biophys. J.* **1984**, *45*, 233. (c) Molle, G.; Duclohier, H.; Spach, G. *FEBS Lett.* **1987**, *224*, 208. (d) Stankowski, S.; Schwarz, U. D.; Schwarz, G. *Biochim. Biophys. Acta* **1988**, *941*, 11. (e) Duclohier, H.; Wroblewski, H. *J. Membr. Biol.* **2001**, *184*, 1. (f) Tieleman, D. P.; Berendsen, H. J.; Sansom, M. S. *Biophys. J.* **2001**, *80*, 331.
(15) Strandberg, E.; Esteban-Martìn, S.; Salgado, J.; Ulrich, A. S. *Biophys. J.* **2009**, *96*, 3223.
(16) Hjørringgaard, C. U.; Pedersen, J. M.; Vosegaard, T.; Nielsen, N. C.; Skrydstrup, T. *J. Org. Chem.* **2009**, *74*, 1329.
(17) Fung, B. M.; Khitrin, A. K.; Ermolaev, K. *J. Magn. Reson.* **2000**, *142*, 97.
(18) Bielecki, A.; Kolbert, A. C.; de Groot, H. J. M.; Griffin, R. G.; Levitt, M. H. *Adv. Magn. Reson.* **1990**, *14*, 111.
(19) (a) Bak, M.; Rasmussen, J. T.; Nielsen, N. C. *J. Magn. Reson.* **2000**, *147*, 296. (b) Tosner, Z.; Vosegaard, T.; Kehlet, C.; Khaneja, N.; Glaser, S. J.; Nielsen, N. C. *J. Magn. Reson.* **2009**, *197*, 120.
(20) Vosegaard, T.; Malmendal, A.; Nielsen, N. C. *Monatsh. Chem.* **2002**, *133*, 1555.
(21) Bak, M.; Schultz, R.; Vosegaard, T.; Nielsen, N. C. *J. Magn. Reson.* **2002**, *154*, 28.

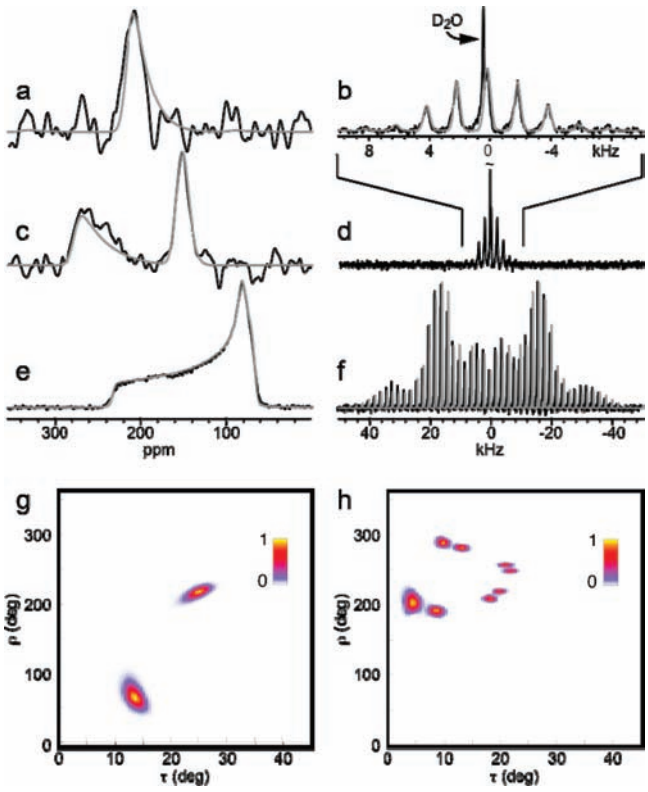

Figure 1. (a,c,e) ^{15}N and (b,d,f) ^{2}H spectra (solid black lines) and corresponding numerical simulations (solid gray lines) forming the basis for our analysis. (a,c) ^{1}H−^{15}N CP experiments of membrane-reconstituted ^{15}N-Aib$_8$-alamethicin uniaxially aligned between glass slides, recorded using ^{1}H (a) SPINAL-64 and (c) FSLG decoupling.[12] (b,d) ^{2}H single-pulse MAS experiment of vesicle-reconstituted ^{2}H-Aib$_8$-alamethicin.[11] (e) ^{15}N static-sample CP and (f) ^{2}H single pulse MAS NMR experiments of lyophilized samples of alamethicin with ^{15}N and ^{2}H labeling, respectively, at position Aib$_8$. (g,h) Restriction plots showing the agreement between the experimental ^{1}H−^{15}N (g) and ^{2}H (h) data in terms of helix tilt angle (τ) and rotational pitch (ρ).

the peptide in consideration may be described in the high-field approximation by[22]

$$H_\lambda = A_{00}^\lambda T_{00}^\lambda + (A_{20}^\lambda)^{\mathrm{L}} T_{20}^\lambda \tag{1}$$

The spatial second-rank, irreducible spherical tensor element $(A_{20}^\lambda)^{\mathrm{L}}$, is calculated via a series of coordinate transformations starting in the principal axis system (P) via the helix system (H), the bilayer system (B), to the lab frame (L). The actual coordinate transformations are performed via Wigner rotations

$$(A_{20}^\lambda)^{\mathrm{L}} = \sum_{m,m',m''=-2}^{2} (A_{2m}^\lambda)^{\mathrm{P}} D_{m,m'}^{(2)}(\Omega_{\mathrm{PH}}) D_{m',m''}^{(2)}(\Omega_{\mathrm{HB}}) D_{m'',0}^{(2)}(\Omega_{\mathrm{BL}}) \tag{2}$$

where $D_{m,m'}^{(2)}(\Omega_{\mathrm{XY}})$ represents the m,m' element of the second-rank Wigner rotation matrix with the Euler angles $\Omega_{\mathrm{XY}} = (\alpha_{\mathrm{XY}},\beta_{\mathrm{XY}},\gamma_{\mathrm{XY}})$ relating the two coordinate systems X and Y. The first transformation from P to H is performed by using knowledge on the typical orientation of the nuclear spin interaction tensors with respect to the peptide plane. We use SIMMOL[21] to define the spatial tensors relative to the molecular geometry as described elsewhere.[20] The H to B transformation represents a rotation of the helical molecule by the Euler angles $\Omega_{\mathrm{HB}} = (\rho,\tau,0)$, where τ describes the helix tilt angle with respect to the bilayer normal and ρ describes the rotational pitch as described elsewhere.[11,12] Under the present experimental conditions (30 °C, 100% relative humidity), the peptides undergo fast rotational diffusion[5,23] around the bilayer normal, leading to a partial averaging of the anisotropic part of the nuclear spin interactions.[11,23,24] This implies that all elements in the sum in eq 2 with $m'' \neq 0$ vanish, leading to the simplified expression for $(A_{20}^\lambda)^{\mathrm{L}}$. In the following expression, we have further used the relations $(A_{2\pm2}^\lambda)^{\mathrm{P}} = -(A_{20}^\lambda)^{\mathrm{P}}\eta_\lambda/\sqrt{6}$ and $D_{0,0}^{(2)}(\Omega_{\mathrm{BL}}) = {}^1/_2(3\cos^2\beta_{\mathrm{BL}} - 1)$, where β_{BL} is the angle between the bilayer normal and the direction of the magnetic field, and η_λ is the asymmetry parameter for interaction λ:

$$(A_{20}^\lambda)^{\mathrm{L}} = \frac{1}{2}(3\cos^2\beta_{\mathrm{BL}} - 1)(A_{20}^\lambda)^{\mathrm{P}} \sum_{m'=-2}^{2} \left(D_{0,m'}^{(2)}(\Omega_{\mathrm{PH}}) - \frac{\eta_\lambda}{\sqrt{6}}[D_{-2,m'}^{(2)}(\Omega_{\mathrm{PH}}) + D_{2,m'}^{(2)}(\Omega_{\mathrm{PH}})] \right) D_{m',0}^{(2)}(\Omega_{\mathrm{HB}}) \tag{3}$$

Now, we introduce a shorthand notation κ to represent the scaling of the nuclear spin interactions upon transformation into the laboratory frame:

$$\kappa(\Omega_{\mathrm{PH}}^\lambda, \eta_\lambda, \Omega_{\mathrm{HB}}) = \sum_{m'=-2}^{2} \left(D_{0,m'}^{(2)}(\Omega_{\mathrm{PH}}^\lambda) - \frac{\eta_\lambda}{\sqrt{6}}[D_{-2,m'}^{(2)}(\Omega_{\mathrm{PH}}^\lambda) + D_{2,m'}^{(2)}(\Omega_{\mathrm{PH}}^\lambda)] \right) D_{m',0}^{(2)}(\Omega_{\mathrm{HB}}) \tag{4}$$

so

$$(A_{20}^\lambda)^{\mathrm{L}} = \frac{1}{2}(3\cos^2\beta_{\mathrm{BL}} - 1)(A_{20}^\lambda)^{\mathrm{P}} \kappa(\Omega_{\mathrm{PH}}^\lambda, \eta_\lambda, \Omega_{\mathrm{HB}}) \tag{5}$$

The Hamiltonian in eq 1 leads to the resonance frequency

$$\nu_\lambda(m) = \langle m|H_\lambda|m\rangle - \langle m-1|H_\lambda|m-1\rangle \tag{6}$$

which, using the expressions from eqs 1 and 5, may be rewritten as

$$\begin{aligned} \nu_\lambda &= \lambda_{\mathrm{iso}} + \lambda_{\mathrm{aniso}}\chi_\lambda \kappa(\Omega_{\mathrm{PH}}^\lambda, \eta_\lambda, \Omega_{\mathrm{HB}}) \frac{1}{2}(3\cos^2\beta_{\mathrm{BL}} - 1) \\ &= \lambda_{\mathrm{iso}} + \lambda_{\mathrm{aniso}}\chi_\lambda \kappa(\rho,\tau) \frac{1}{2}(3\cos^2\beta_{\mathrm{BL}} - 1) \end{aligned} \tag{7}$$

with the introduction of the magnitude of the nuclear spin interactions λ_{aniso} (C_{Q}, δ_{aniso}, and b_{IS} for the quadrupole coupling, chemical shift, and dipole−dipole interactions, respectively), the interaction- and pulse sequence-dependent parameter χ_λ, and, in the lower part of the equation, the shorthand notation $\kappa(\rho,\tau) = \kappa(\Omega_{\mathrm{PH}}^\lambda,\eta_\lambda,\Omega_{\mathrm{HB}})$ emphasizing only the interesting parametric dependences of κ. χ_λ includes constants from the nuclear spin interactions as well as pulse-sequence specific scaling factors. The latter is relevant for FSLG decoupling, which gives a scaling of the heteronuclear dipole−dipole coupling of $1/\sqrt{3}$. Values for χ_λ and the nuclear spin interaction parameters are listed in Table 1. For bilayer samples with no orientational preference (e.g., vesicle-reconstituted peptide samples), we may interpret the powder pattern in terms of a reduced interaction with the following properties: $\lambda_{\mathrm{iso}}^{\mathrm{red}} = \lambda_{\mathrm{iso}}$, $\lambda_{\mathrm{aniso}}^{\mathrm{red}} = \lambda_{\mathrm{aniso}}\kappa(\rho,\tau)$, $\eta_\lambda^{\mathrm{red}} = 0$.

Equipped with these equations, we may analyze the experimental spectra in Figure 1 to determine the experimental scaling factors, $\kappa_\lambda^{\mathrm{exp}}$. These scaling factors are obtained by measuring experimental

(22) Ernst, R. R.; Bodenhausen, G.; Wokaun, A. *Principles of Nuclear Magnetic Resonance in One and Two Dimensions*; Calendron Press: Oxford, 1987.

(23) Cady, S. D.; Goodman, C.; Tatko, C. D.; DeGrado, W. F.; Hong, M. *J. Am. Chem. Soc.* **2007**, *129*, 5719.

(24) Prongidi-Fix, L.; Bertani, P.; Bechinger, B. *J. Am. Chem. Soc.* **2007**, *129*, 8430.

Table 1. Experimental Values for the ^{2}H Quadrupole Coupling (C_Q, η_Q), ^{15}N Anisotropic Chemical Shift (δ_{iso}, δ_{aniso}, η_σ), and ^{1}H−^{15}N Dipole−Dipole Coupling (b_{IS})

interaction	λ_{iso}	λ_{aniso}	η_λ	χ_λ
^{2}H quadrupole coupling[a]		53.1 ± 2.1 kHz	0	±3/4
^{15}N chemical shift anisotropy[b]	126 ± 2 ppm	104 ± 2 ppm	0.14 ± 0.05	1
^{1}H−^{15}N dipole−dipole coupling[c]		10.4 kHz		$\pm 1/\sqrt{3}$

[a] The ^{2}H quadrupole coupling parameters have been determined from the experimental spectrum in Figure 1f. [b] The ^{15}N CSA parameters have been determined from the experimental spectrum in Figure 1e. [c] This ^{1}H−^{15}N dipole−dipole coupling corresponds to a H−N bond length of 1.05 Å, which is typically observed in proteins in lipid bilayers.[29] The scaling factor of $\pm 1/\sqrt{3}$ originates from the fact that FSLG decoupling gives a scaling factor of $1/\sqrt{3}$ for the heteronuclear dipole−dipole coupling.

Table 2. Experimental Scaling Factors from ^{2}H and ^{1}H−^{15}N Solid-State NMR Experiments of Alamethicin with ^{2}H or ^{15}N Labels at Aib$_8$[a]

interaction	parameter	κ_λ^{exp}	$\Delta\kappa_\lambda$	reference
^{2}H quadrupole coupling[b]	κ_{Q1}^{exp}	0.19 ± 0.03	0.04	11
	κ_{Q2}^{exp}	0.13 ± 0.02	0.04	11
^{15}N chemical shift anisotropy[c]	κ_σ^{exp}	0.85 ± 0.05	0.06	12
^{1}H−^{15}N dipole−dipole coupling[d]	κ_{Dip}^{exp}	0.43 ± 0.03	0.04	12

[a] The data were obtained using either static experiments on oriented bilayer samples or MAS experiments on vesicle samples. The values for $\Delta\kappa_\lambda$ are generally larger than the experimental error limits to compensate for uncertainties not included in the experimentally determined parameters, for example, the $C^{\beta 1}-C^\alpha-C^{\beta 2}$ bond angle, or the exact H−N bond length. [b] The quadrupole coupling scaling factors are calculated from the experimental values in Table 1 and the reduced quadrupole coupling parameters: $C_{Q1}^{red} = 6.7 \pm 0.8$ kHz, and $C_{Q2}^{red} = 10.0 \pm 1.5$ kHz.[11] [c] The chemical shift scaling factor is calculated from the experimental values in Table 1 and the observed frequency $\delta_{obs} = 214 \pm 2$ ppm in the spectrum of the bilayer sample. [d] The dipole−dipole coupling scaling factor has been calculated assuming a NH-bond length of 1.05 Å corresponding to a dipole−dipole coupling of $b_{IS} = 10.4$ kHz and using an observed splitting of 7411 ± 500 Hz in the ^{1}H FSLG-decoupled ^{15}N spectrum compensated by the theoretic scaling factor leading to $\chi_{Dip} = \pm 1/\sqrt{3}$ (cf., eq 7).

values for either ν_λ or λ_{aniso}^{red} from data reported elsewhere,[11,12] as summarized in Table 2.

Restriction Plots. Orientational constraints from solid-state NMR experiments as described above may be represented as so-called restriction plots[25] showing which molecular conformations are compatible with the measurements. We will use the convenient description ($\kappa_\lambda(\rho,\tau)$) to define the restriction score (R) by the following Gaussian function:

$$R_\lambda(\rho,\tau) = \exp\left\{-4 \ln 2\left(\frac{\kappa_\lambda^{exp} - \kappa_\lambda(\rho,\tau)}{\Delta\kappa_\lambda}\right)^2\right\} \qquad (8)$$

where $\Delta\kappa_\lambda$ is the estimated uncertainty for the particular measurement that determines the tightness of the restriction. Using this setting, Figure 1g and h shows the restriction plots for the ^{2}H quadrupole coupling and ^{15}N chemical shift/^{1}H−^{15}N dipolar coupling data, respectively. These are plots of $R_\lambda(\rho,\tau)$ as a function of ρ and τ using the experimental parameters (κ_λ^{exp}, $\Delta\kappa_\lambda$) listed in Table 2 assuming a static anchoring model. A high value (maximum 1) represents a good agreement between the model and experimental data, while a low value (minimum 0) represents poor agreement. Both restriction plots in Figure 1 are in agreement with a small tilt angle of 5−10° but do not agree on the rotational pitch angle.

MD Simulations. An all-atom molecular system was built from 25 alamethicin peptides and 330 DMPC lipids and hydrated with water. After equilibration for 1.2 ns, the system was converted to a coarse-grained (CG) representation and subjected to three independent MD simulations, each for 1 μs. The details of the setup and the simulations are reported elsewhere.[13]

The helix tilt angle of a peptide was defined as the angle between the membrane normal (the z axis) and the "helix axis" determined from the position of the backbone beads of residues 7, 8, and 9 using the procedure to establish helix directions for cylinder representations in MolScript.[26] The rotation angle of a peptide was defined as the angle between the plane spanned by the "helix axis" and the z axis (defined as the zero-point for the rotation) and the axis going perpendicularly from the "helix axis" through the center-of-mass of the two side-chain beads of Aib$_8$ in the CG representation.

Results and Discussion

Dynamic Anchoring Model. Our target molecule is alamethicin for which we focus on the helical region of the molecule between the highly conserved Gln$_7$, assumed to play a central role in the channel-conductance of the molecule, and the flexible hinge formed by Gly$_{11}$ to Pro$_{14}$. With reference to the strong helix promoting properties of Aib[27] and our ability to label such residues with ^{2}H on the two methyl groups and ^{15}N in the amide position, we probe the dynamics of a helical fragment in the N-terminal part of alamethicin through investigation of the dynamics of Aib$_8$ by simultaneous analysis of the orientation-dependent ^{15}N chemical shift, ^{1}H−^{15}N dipole−dipole coupling, and ^{2}H quadrupole coupling tensors for this residue.[11,12] The helix-promoting properties of Aib, due to the steric constraints caused by the two side-chain methyl groups that both point away from the molecular structure, are reflected by a narrow distribution of backbone torsion angles for Aib residues in α-helical environments for earlier reported peptaibol structures. Such an analysis shows average torsion angles of $\varphi = -55 \pm 5°$, $\psi = -45 \pm 7°$, with the error limits representing the standard deviation among 72 different residues in 10 peptaibol structures.[28] These values are close to the values generally observed in transmembrane α-helices ($\varphi = -60°$, $\psi = -45°$).[8,29,30]

Based on the general helix-promoting properties of Aib, the well-established fact that the N-terminal part of alamethicin forms an α-helix structure,[9,31] and the narrow distribution of torsion angles observed for Aib in α-helix structures, we assume that Aib$_8$ adopts the α-helical torsion angles $\varphi = -55°$, $\psi = -45°$. These torsion angles imply that the residues Gln$_7$-Aib$_8$-Val$_9$ form an α-helical segment, which makes it most relevant to use a structural and dynamic model where the helix segment around Aib$_8$ is specified by its average helix tilt (τ) and rotation angles (ρ) around which the helix segment wobbles very fast with motions described by amplitudes of $\Delta\tau$ and $\Delta\rho$. Assuming that the wobbling is fast relative to the NMR time scale, the resulting NMR resonances will be sharp lines positioned at the weighted average frequency of the different molecular conformations. To include the effect of such fast dynamics in the

(25) Bechinger, B.; Zasloff, M.; Opella, S. J. *Protein Sci.* **1993**, *2*, 2077.
(26) Kraulis, P. J. *J. Appl. Crystallogr.* **1991**, *24*, 946.
(27) Banerjee, R.; Basu, G.; Roy, S.; Chène, P. *J. Pept. Res.* **2002**, *60*, 88.
(28) Whitmore, L.; Wallace, B. A. *Nucleic Acids Res.* **2004**, *32*, D593.
(29) Wang, J.; Kim, S.; Kovacs, F.; Cross, T. A. *Protein Sci.* **2001**, *10*, 2241.
(30) Kim, S.; Cross, T. A. *Biophys. J.* **2002**, *83*, 2084.
(31) Fox, R. O., Jr.; Richards, F. M. *Nature* **1982**, *300*, 325.

analysis of orientational constraints from solid-state NMR, we assume that the dynamics of the helix segment may be described by Gaussian fluctuations of the helical peptide around its helix axis, corresponding to variations in the rotational pitch ($\Delta\rho$), as well as fluctuations in the helix tilt ($\Delta\tau$). We let $\Delta\rho$ and $\Delta\tau$ denote the half-width at half height (HWHH) of the Gaussian distributions. Using this dynamic model, we may calculate the average scaling factor by integration over the Gaussian distributions:

$$\bar{\kappa}_\lambda(\rho,\tau,\Delta\rho,\Delta\tau) = \frac{\ln 2}{\pi\Delta\rho\Delta\tau}\int_{-\infty}^{\infty}\int_{-\infty}^{\infty}\kappa(\rho+r,\tau+t)\exp\left\{-\ln 2\left(\left(\frac{r}{\Delta\rho}\right)^2+\left(\frac{t}{\Delta\tau}\right)^2\right)\right\}\mathrm{d}r\,\mathrm{d}t \qquad (9)$$

In this equation, the integration of r and t should in principle go from $-\infty$ to $+\infty$, but in the numerical implementation, we have found that integration in the range $-3\Delta\rho \le r \le 3\Delta\rho$ and $-3\Delta\tau \le t \le 3\Delta\tau$ in steps of 1° ensures convergence of the integral. In the limit $\Delta\rho \to 0$, the corresponding integral over r disappears, and we only evaluate the function $\kappa(\rho,\tau + t)$, likewise, for the t-integral if $\Delta\tau \to 0$. Having calculated the average scaling factor $\bar{\kappa}_\lambda(\rho,\tau,\Delta\rho,\Delta\tau)$, we may calculate the restriction plot (R_λ) where $\bar{\kappa}_\lambda(\rho,\tau,\Delta\rho,\Delta\tau)$ substitutes $\kappa_\lambda(\rho,\tau)$ in eq 8.

To extend this description, we may define order parameters for the molecular fluctuations around the helix axis, S_ρ^2, corresponding to $\Delta\rho$, and perpendicular to the helix axis, S_τ^2, corresponding to $\Delta\tau$. Instead of making a full expansion of the second-rank tensorial interactions,[32] we use a simple representation where explicit expressions for the transformation of a second-rank tensor have been replaced with cosine terms leading to

$$S_\rho^2 = \frac{\sqrt{\ln 2}}{\sqrt{\pi}\Delta\rho}\int_{-\infty}^{\infty}\exp\left\{-\ln 2\left(\frac{r}{\Delta\rho}\right)^2\right\}\cos r\,\mathrm{d}r = \exp\left\{-\frac{(\Delta\rho)^2}{4\ln 2}\right\} \qquad (10)$$

$$S_\tau^2 = \frac{\sqrt{\ln 2}}{\sqrt{\pi}\Delta\tau}\int_{-\infty}^{\infty}\exp\left\{-\ln 2\left(\frac{t}{\Delta\tau}\right)^2\right\}\cos 2t\,\mathrm{d}t = \exp\left\{-\frac{(\Delta\tau)^2}{\ln 2}\right\} \qquad (11)$$

so the order parameters range from 0 to 1. In these definitions, $\Delta\rho$ and $\Delta\tau$ are given in radians.

Dynamics in Simulated PISA Wheels. The spectroscopic signatures of ideal uniformly ^{15}N-labeled α-helices in 2D ^{1}H−^{15}N dipolar/^{15}N chemical shift correlation experiments, the so-called PISA wheels,[2] have provided a fast way to interpret the otherwise quite complex spectra from uniformly labeled proteins. Interestingly, the current dynamics model significantly changes the resonance positions in such PISA wheels, as visualized in Figure 2. Upon inspection of the dynamics-induced change of the PISA wheel shapes, some trends are actually quite intuitive: (i) Increase of $\Delta\rho$ decreases the diameter of the wheel, and in the case of very large rotational fluctuations all of the resonances in the wheel are indistinguishable. (ii) Increase of $\Delta\tau$ moves the wheel toward the isotropic shift (and zero dipolar coupling) because the dynamic fluctuations average out the anisotropy, and also slightly decreases the diameter of the wheel. (iii) The fact that the PISA wheels shrink toward their "center-of-mass" when increasing $\Delta\rho$ implies that the resonances with large dipolar couplings display reduced couplings, while those with small dipolar couplings display increased couplings. The latter observation is somewhat surprising in the sense that traditional order-parameter models always reduce the strength of the nuclear spin interactions.

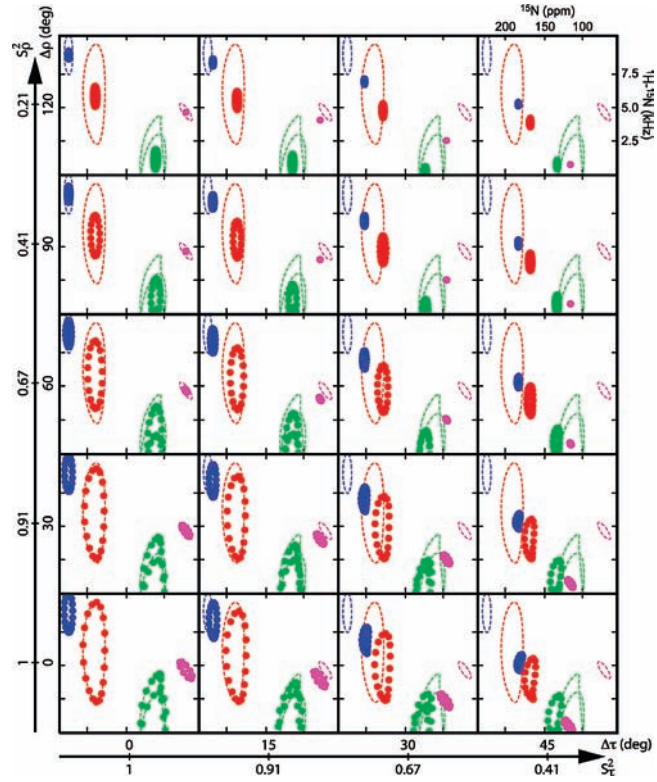

Figure 2. Simulated PISA wheels for ^{1}H−^{15}N SLF experiments of an α-helical peptide (torsion angles $\varphi = -55°$, $\Psi = -45°$, H−N bond length 1.05 Å) with different degrees of conformational dynamics as expressed by $\Delta\rho$ and $\Delta\tau$ or S_ρ^2 and S_τ^2 (filled circles) and without dynamics (dashed lines). The wheels represent τ values of 10° (blue), 30° (red), 60° (green), and 90° (magenta).

Characterization of Residue-Specific Dynamics Information. While inclusion of dynamics in the PISA wheel simulations leads to remarkably different wheel patterns depending on $\Delta\rho$ and $\Delta\tau$, the investigation of dynamics in PISA wheels from SLF experiments requires the assumption of a well-defined secondary structure for a sufficiently large fragment of the protein to define the wheel shape.[8,15] In the present work, we will contrast this by performing the investigation of dynamics on the residue level, from the complementary constraints of the ^{15}N backbone amide and ^{2}H labeling of the methyl groups of Aib_8 in alamethicin.

Using the same dynamic model as above, with fluctuations in the helix tilt and rotational pitch described by $\Delta\tau$ and $\Delta\rho$, respectively, as accounted for by $\bar{\kappa}_\lambda(\rho,\tau,\Delta\rho,\Delta\tau)$, the parameter space spanned by these four variables is investigated in the grid of ρ,τ-restriction plots in Figure 3 featuring different values for dynamics half-width parameters $\Delta\rho$ and $\Delta\tau$. Each tile in Figure 3 represents a restriction plot calculated using the values in Table 2. Specifically, Figure 3a and b shows the ^{15}N and ^{2}H restriction plots, while Figure 3c shows the product of these restriction plots, which represents the combined restriction from these data.

(32) (a) Clarke, J. B.; Hastie, J. W.; Kihlborg, L. H. E.; Metselaar, R.; Thackeray, M. M. *Pure Appl. Chem.* **1994**, *66*, 577. (b) Cavanagh, J.; Fairbrother, W. J.; Palmer, A. G., III; Skelton, N. J. *Protein NMR Spectroscopy: Principles and Practice*; Academic Press: New York, 1995.

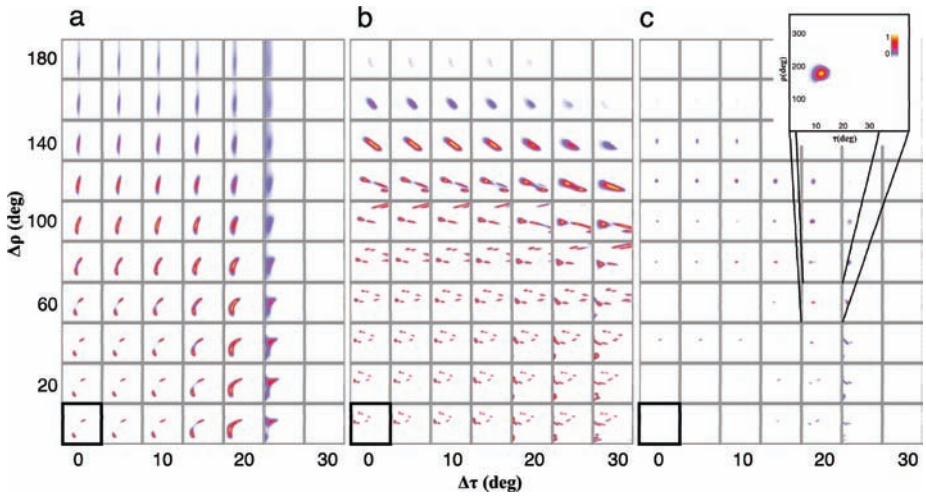

Figure 3. Restriction plots for (a) the $^{1}H-^{15}N$ and (b) ^{2}H data in Figure 1 along with (c) the combined (product of (a) and (b)) restriction plots for various values of $\Delta\rho$ and $\Delta\tau$. Each restriction plot represents helix tilt angles (horizontal) and rotational pitch angles (vertical) in the range $0° \tau \leq 45°$ and $0° \leq \tau \leq 360°$. There is no significant intensity in the restriction plots with $\tau > 45°$. The highlighted tiles in the lower-left corners correspond to the static anchoring case $\Delta\tau = \Delta\rho = 0°$. The color coding in the restriction plots corresponds to that used in Figure 1g and h (blue means low restriction score (close to 0), and yellow means high restriction score (close to 1)).

Within the proposed helix dynamics model, we first inspect the special case of no dynamics ($\Delta\rho = \Delta\tau = 0$, the lower left framed tiles in Figure 3). From these restriction plots (of which the $^{1}H-^{15}N$ and ^{2}H restriction plots are identical to those in Figure 1g and h), it is evident that a static model does not describe the data convincingly, because the combined restriction plot does not show regions with mutual agreement. However, when focusing on structural models with substantial fluctuations in the membrane anchoring, we observe a good agreement between the two data sets, as it was observed that the conformational regions are in agreement with the combined restriction.

To inspect the exact modes of dynamics in terms of $\Delta\rho$ and $\Delta\tau$, Figure 4a reports the maximum score of each combined restriction plot (from Figure 3c, but in a finer grid) as a function of $\Delta\rho$ and $\Delta\tau$. We observe a continuum of solutions yielding three curved ridges of which two have higher restriction scores, one starting at $\Delta\tau,\Delta\rho = 0°,95°$ ending at $\Delta\tau,\Delta\rho = 23°,0°$ (marked by † in Figure 4a) and one starting at $\Delta\tau,\Delta\rho = 0°,38°$ ending at $\Delta\tau,\Delta\rho = 19°,0°$ (marked by ‡ in Figure 4a). Expressed in terms of the order parameters introduced in eqs 10 and 11, the plot reveals that the solid-state NMR data are in agreement with conformational order parameters as small as $S_\tau^2 \approx 0.8$ and $S_\rho^2 \approx 0.4$. To investigate which molecular conformations give rise to these two ridges, we have inspected the source restriction plots with a maximum restriction score above 0.5 (arbitrary value that includes both ridges and corresponds to $|\kappa_\lambda - \kappa_\lambda^{exp}| < \Delta\kappa_\lambda/2$). When plotting the τ,ρ values providing the maximum score in these restriction plots belonging to these ridges as illustrated in Figure 4b, we observe that the maximum scores of the †-ridge correspond to molecular conformations given by $\tau = 10-20°$ and $\rho \approx 170°$, while those of the ‡-ridge correspond to the region $\tau = 16-23°$ and $\rho \approx 210°$.

Conformation Probability Plots. To combine the information from the τ,ρ-restriction plots with the information about $\Delta\tau$ and $\Delta\rho$, we have chosen to represent the data as plots where the τ,ρ-restriction plots are broadened by convolution of the restriction plot with a Gaussian function with a HWHH corresponding to the respective values for $\Delta\tau$ and $\Delta\rho$, and finally normalized to a total probability of 1. Such plots will henceforth be referred to as conformation probability plots, as they will represent the probability of finding the helix segment in a certain conformation according to our Gaussian model based on the $^{1}H-^{15}N$ and ^{2}H solid-state NMR data. Because we do not observe a single solution in the $\Delta\tau,\Delta\rho$ plot, we assume the continuum solution including conformations for which $|\kappa_\lambda - \kappa_\lambda^{exp}| < \Delta\kappa_\lambda/4$ (restriction scores larger than 0.84) corresponding to the high values in the †- and ‡-ridges. We process each restriction plot individually by the convolution procedure described above. The resulting conformation probability plot shown in Figure 5a displays significant molecular dynamics with respect to both helix tilt and rotational pitch as evidenced by

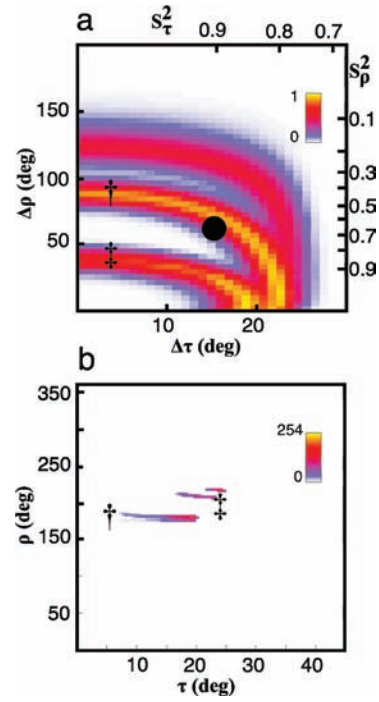

Figure 4. (a) Maximum score in the combined restriction plots as a function of $\Delta\tau$ and $\Delta\rho$ or S_τ^2 and S_ρ^2. The possible solution falls on two distinct ridges labeled † and ‡. The black dot indicates the point $\Delta\tau = 15°$, $\Delta\rho = 56°$ being in agreement with the coarse-grained MD simulation. (b) Sum of the maximum score in all restriction plots (for different $\Delta\tau$, $\Delta\rho$ values) with scores larger than 0.5.

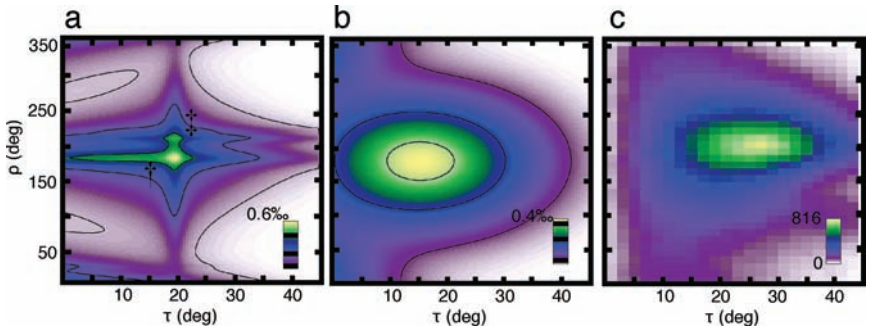

Figure 5. Conformation probability plots obtained by convolution of the restriction plot with a Gaussian broadening function corresponding to the value for $\Delta\rho$ and $\Delta\tau$. (a) Conformation probability plot from all restriction plots with restrictions scores larger than 0.84 (colored yellow in Figure 4a), each broadened corresponding to their $\Delta\rho$ and $\Delta\tau$ values, and subsequently added. (b) Conformation probability plot from the restriction plot indicated by a black dot in Figure 4a ($\Delta\tau = 15°$, $\Delta\rho = 56°$). (c) Conformation counts of Aib_8 in alamethicin in hydrated bilayers from a coarse-grained MD simulation (see text for details). The contours in (a) and (b) enclose molecular conformations with more than 95%, 50%, and 10% probability.

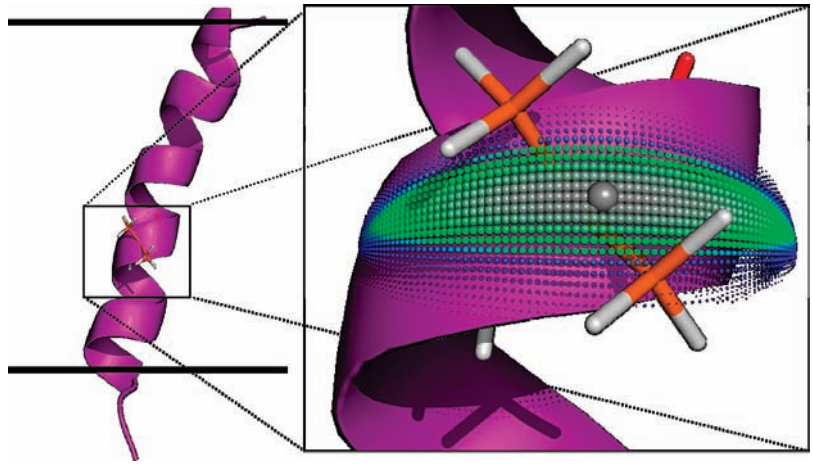

Figure 6. Visualization of the dynamic behavior of Aib_8 in alamethicin in the membrane in terms of helix motion. The monomer structure recently determined by solution-state NMR and MD simulations in isotropic bicelles[9] is positioned in agreement with average helix tilt and rotational pitch angles determined here, with the thick bars indicating the orientation of the phospholipid bilayer. The large gray sphere in the expansion indicates the center of mass of the two C^β atoms, while the gray, green, and blue spheres correspond to conformations in the conformation probability plot (Figure 5b) using the same color coding and with their diameter reflecting the probability.

the observation of molecular excursions in the range $-5° < \tau < 35°$ and $100° < \rho < 210°$. Specifically, the contour lines enclose the molecular conformations with 95%, 50%, and 10% occupancy.

At present, there are no complementary experimental data to support our dynamic model for the membrane anchoring of alamethicin, although we recently demonstrated the highly dynamic nature of the peptide−lipid interactions by liquid-state NMR.[9] Thus, we have chosen to compare the present experimental results in the conformation probability plot with the results from three independent CG MD simulation using 25 alamethicin molecules in a hydrated lipid bilayer with a peptide/lipid ratio similar to that used for the experiments.[13] For 2000 time frames (equally distributed from 200 to 1000 ns) for each of the three MD simulations, we have calculated the helix tilt and rotational pitch angles for the residues framing Aib_8 in all alamethicin molecules and plotted the counts in Figure 5c. This plot shows which conformations are most occupied and thus relates directly to the conformation probability plots introduced above. The plot shows a quite homogeneous distribution around a conformation corresponding to $\tau,\rho = 25°,200°$ and matches well with a Gaussian distribution width of $\Delta\tau,\Delta\rho = 15°,56°$ (highlighted by a black dot in Figure 4a). While the agreement between the counts in Figure 5c and the unbiased conformation probability plot in Figure 5a is relatively good, we do note that the MD simulations shows larger variations in ρ but smaller variations in τ than the conformation probability plot in Figure 5a.

We note that the Gaussian distribution for the conformations from the MD simulations leads to values ($\Delta\tau,\Delta\rho = 15°,56°$) that are located near the †-ridge in Figure 4a (with a restriction score of 0.82). To investigate this finding in more detail, Figure 5b reports the conformation probability plot corresponding to these values. Considering the large motional excursions undertaken by the molecule, small variations in the average conformation between MD and NMR are expected, so we conclude that there is a very good agreement between the conformation probability plot from the NMR data (Figure 5a and b) and the MD conformation plot (Figure 5c), although the average molecular conformation differs slightly from MD to NMR, particularly the tilt being determined to $\tau = 16°$ from the solid-state NMR data and $\tau = 25°$ from MD.

To visualize the results of the dynamics model, Figure 6 shows an alamethicin molecule[9] highlighting the backbone and methyl groups of Aib_8. The figure illustrates the motion of the helical segment around Aib_8 by a gray sphere placed at the center-of-mass of the two C^β atoms surrounded by a large number of smaller spheres colored in gray, green, and blue. These spheres represent the conformational excursions of the

center-of-mass within the $\Delta\tau,\Delta\rho$ space corresponding to the conformation probability plot in Figure 5b using the same color code. In this visualization, it becomes clear that the helix fragment around Aib_8 of alamethicin undergoes significant molecular motion, in agreement with the results of the MD simulations.

Discussion of Dynamic Models. Our model for the dynamics of the peptide, based on the Gaussian distribution introduced in eq 9, assumes that motion described by changes in helix tilt and rotational pitch are uncorrelated. Yet, studies of more constrained molecular structures, for example, RNA, have demonstrated highly correlated modes of motion.[33] In the present study, it would also be reasonable to expect some degree of correlation between helix tilt and rotational pitch if, for example, the alamethicin molecules were anchored more tightly in the C-terminal end and the dynamics were due to variable kinks in the flexible Gly_{11}-X-X-Pro_{14} region.[34] Our recent liquid-state NMR and MD studies provided experimental insight into this helix kink,[9] but could not determine the tightness of the anchoring of the C terminal. The coarse-grained MD simulations provide no sign of correlation between the helix tilt and rotational pitch as evidenced by the Gaussian appearance of the helix conformation plot in Figure 5c. Interestingly, the MD data show a more loose binding of the C-terminal part (determined from a helix conformation plot of Aib_{16}, data not shown) as also suggested in the early model of Fox and Richards.[31] Inclusion of more complex coupled modes of motion in a de novo characterization of the molecular dynamics would require more experimental constraints, including data from, for example, ^{13}C NMR experiments on $^{13}C^{\alpha}$- or $^{13}C'$-labeled samples. An alternative approach to the de novo characterization could be to include the solid-state NMR constraints in restrained MD simulations using ensemble averaging similarly to the approach of Lindorff-Larsen et al.[35] A detailed analysis and implementation of this approach is beyond the scope of this Article, but is currently subject to further investigation.

Our experimental data clearly demonstrate that important new insight into the conformational flexibility of proteins with respect to their incorporation into biological membranes may be achieved from solid-state NMR experiments. It is evident that the membrane anchoring of alamethicin is highly flexible, which from an overall point of view is in agreement with previous observations, for example, of Salditt and co-workers,[36] but at the same time in strong contrast to the apparently more well-defined membrane-bound conformations of other antimicrobial peptides like magainin 2.[37] More importantly, it opens up new possibilities to challenge current models for the action of, for example, antimicrobial peptides and their ability to sample structures competent for antimicrobial activity. The wobbling (back-forth rotation, and variable tilting) of alamethicin, as represented graphically in Figure 6, may provide information not only about the interaction between alamethicin and the surrounding membranes, but also about alamethicin−alamethicin interactions and channel formation. Determinants for the range of dynamics may be the amphiphatic character of the molecule enabling formation of a multimeric alamethicin pore structure, as well as the mixture of hydrophilic and hydrophobic side chains for the N- and C-terminal residues and may render partial rotation and limited variation of the tilt angle around ~20° in a transmembrane arrangement plausible when considered in a rigid-body motional model.[3] A relatively modest variation in the rotational pitch angles may provide insight into the specific arrangements of molecules in a multimeric channel, and variations in the tilt angle may mediate ion transport and membrane thinning. In a more detailed view, the ability of the proposed method to provide residue-specific information may allow experimental "in-situ" exploration of details of channel formation in a more "unordered" and flexible arrangement as discussed previously.[12,13,36,38]

Focusing on the ability to characterize the dynamics at the residue-specific level, such insight is of great interest for flexible molecules like alamethicin, where previous studies have demonstrated the highly dynamic nature of the peptide[13] and even suggest that its interaction with the lipids and solvent and thereby the local dynamics vary significantly throughout the peptide chain.[9]

To achieve such detailed information, a large number of structural constraints is needed for the target residues. We have benefitted from studying Aib, for which we may achieve four structural constraints from $^1H-^{15}N$ and ^2H data. If we were to study other residues, it would be obvious to turn to ^{13}C labeling of either C' or C^{α} and use chemical shift and dipole−dipole coupling restraints from these nuclei in addition to the $^1H-^{15}N$ data.[39] Thus, it would be a feasible task to perform a detailed dynamic analysis of all residues in a peptide.

Conclusion

We have demonstrated that it is possible to use the complementary information from backbone ^{15}N and side-chain ^2H solid-state NMR data to set up a detailed residue-specific dynamic model for the membrane anchoring of membrane-bound peptides. The experimental results achieved for the peptaibol alamethicin are in excellent agreement with the corresponding dynamic model from a coarse-grained MD simulation of an ensemble of alamethicin molecules in hydrated lipid bilayers. This new approach opens the possibility to study the local dynamics of peptides at the residue-specific level, thus providing insight into both the overall motion of the molecule and the internal modes of motion.

Acknowledgment. Support from the Danish National Research Foundation, the Danish Natural Science Research Council, Lundbeckfonden, the Danish Center for Scientific Computing (DCSC), and the Danish Biotechnology Instrument Centre (DABIC) is acknowledged.

JA908604U

(33) Zhang, Q.; Stelzer, A. C.; Fisher, C. K.; Al-Hashimi, H. M. *Nature* **2007**, *450*, 1263.
(34) Tieleman, D. P.; Shrivastava, I. H.; Ulmschneider, M. R.; Sansom, M. S. P. *Proteins* **2001**, *44*, 63.
(35) Lindorff-Larsen, K.; Best, R. B.; DePristo, M. A.; Dobson, C. M.; Vendruscolo, M. *Nature* **2005**, *433*, 128.
(36) (a) Spaar, A.; Münster, C.; Salditt, T. *Biophys. J.* **2004**, *87*, 396. (b) Li, C.; Salditt, T. *Biophys. J.* **2006**, *91*, 3285.
(37) (a) Bechinger, B.; Zasloff, M.; Opella, S. J. *Biophys. J.* **1992**, *62*, 12. (b) Matsuzaki, K. *Biochim. Biophys. Acta* **1998**, *1376*, 391.
(38) Cascio, M.; Wallace, B. A. *Proteins* **1988**, *4*, 89.
(39) Sinha, N.; Grant, C. V.; Park, S. H.; Brown, J. M.; Opella, S. J. *J. Magn. Reson., Ser. B* **2007**, *186*, 51.